DAMAGE EVOLUTION IN SHORT FIBRE REINFORCED POLYAMIDE CAUSED BY BIAXIAL LOADING

K. Metzkes[1], V. Trappe*[1]

[1] *BAM Federal Institute for Materials Research and Testing, Unter den Eichen 87, 12205 Berlin, Germany*

* *Corresponding Author: volker.trappe@bam.de*

Keywords: short fibre reinforced composites, multiaxial loading, non-destructive testing, damage evolution, damage state

Abstract

The multiaxial fatigue damage behaviour of short fibre reinforced polyamide 6 is analysed on injection moulded tube samples. In parallel with the fatigue tests, the damage state is evaluated nondestructively by X-ray refraction analysis which detects inner surfaces by the variation of electron density. By applying X-ray refraction analysis and a model based on [1] by GÜNZEL *the micro damage evolution can be separated into fibre matrix debonding and matrix-micro cracking.*

1. Introduction

In automotive applications short fibre reinforced polyamide is increasingly used because of its properties regarding light weight design, recyclability and cost efficient manufacturing by injection moulding. For an effective design process and the application in safety related components it is necessary to understand the damage behaviour of the anisotropic material due to multiaxial loadings. This publication deals with the biaxial fatigue damage behaviour of short fibre reinforced polyamide (PA6 GF30). Firstly the uniaxial and biaxial fatigue behaviour of the load ratios $R = 0.1$, $R = 10$ and $R = -1$ is characterised. Secondly the micro damage evolution caused by fatigue loading is focused on. Since the occurring damage phenomena in short fibre reinforced thermoplastics depend on the fibre orientation distribution and the applied load, the nondestructive and directional detection of inner surfaces by X-ray refraction analysis provides the potential to characterize the evolution of damage. For uniaxial loadings the damage mechanisms of this material has been studied by GÜNZEL in [1] and TRAPPE et.al. in [2]. Based on this model the separation of micro damage phenomena with respect to the global fibre orientation is possible.

2. Theory

2.1. Damage phenomena

The damage behaviour of short fibre reinforced plastics is ascribed to the micro damage phenomena of debonding in the fibre-matrix-interface, fracture of fibres and matrix-micro-cracking

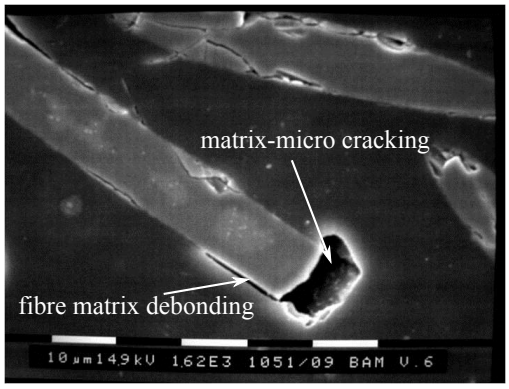

Figure 1. Micro damage phenomena in short fibre reinforced polyamide

(figure 1). The qualitative and quantitative occurrence of these phenomena depends on the stress state and on the load direction in relation to the fibre orientation. In the present paper the fibre-matrix-debonding and the matrix-micro-cracking caused by tension and torsion fatigue loading is focused on.

2.2. X-ray refraction analysis

X-rays are refracted at interfaces of media or material where the electron density changes. This effect is comparable to the refraction of visible light at glass lenses. The method of X-ray refraction analysis, which is based on small angle X-ray scattering (SAXS) uses this effect [3, 4]. In figure 2 the experimental setup of the X-ray refraction experiment is shown. The X-ray beam

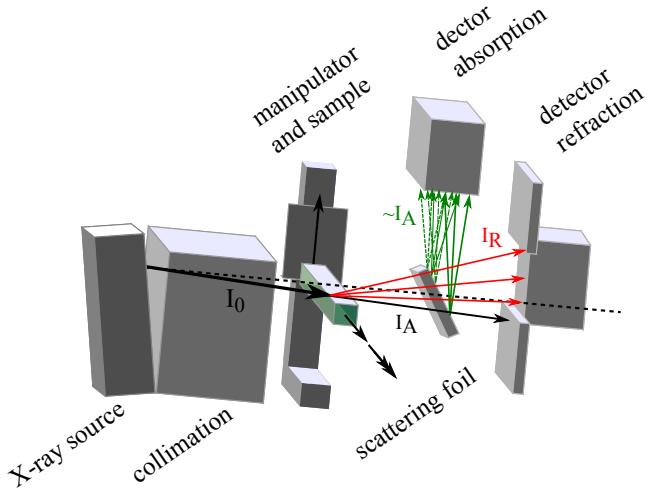

Figure 2. Experimental setup of the X-ray refraction topography

($Mo - K\alpha$, $\lambda = 0.7$ Å) which is collimated to a rectangular square section ($1 - 2 \times 0,05$ mm) by a *Kratky*-collimation, passes the sample. The intensity of absorption I_A is measured indirectly by a scattering foil and the intensity of refraction I_R is measured directly. These intensities as well as their zero values I_{A0} ans I_{R0}, measured without a sample in the path of rays, lead to the refraction value C (eq. 1), which represents the inner surface of the radiographed volume. The

absorption is described by LAMBERT-BEER-Law (eq. 2). From (eq. 1) and (eq. 2) follows the specific refraction value C/μ which is independent from the materials thickness.

$$C = \left[\frac{I_R/I_{R0}}{I_A/I_{A0}} - 1 \right] \cdot d^{-1} \tag{1}$$

$$I_A = I_{A0} \cdot e^{-\mu \cdot d} \tag{2}$$

Glass fibres with the shape of cylindrical lenses cause a refraction of X-rays in a plane perpendicular to the fibre axis. Therefore the orientation of fibres can be measured by X-ray refraction topography [5, 6]. In composite materials three types of inner surfaces appear: Bonded fibre, debonded fibres and matrix cracks. Assuming bonded fibre cladding and debonded end faces in the undamaged state, the integral and plane fibre orientation can be determined. Progressive damage is caused by the debonding of fibres and matrix micro-cracking, that results in an increase of the refraction value ΔC (eq. 3). Due to the homogeneous distribution of inner surfaces in the PA6 GF30 the mean value C_m of a representative volume is used. [1, 2, 7, 8]

$$\Delta C_{mi} = \frac{C_{mi} - C_{m0}}{C_{m0}} \qquad i = \text{load step} \tag{3}$$

3. Material and test samples

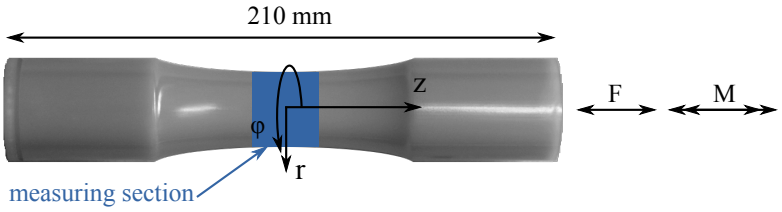

Figure 3. Tube sample (PA6 GF30)

This study analyses a polyamide 6 with 30 % by weight (≈ 15 % by volume) of short glass fibre reinforcement for injection moulding applications (uncolored B3WG6 by Co. BASF SE). The fibre length is WEIBULL-distributed with an average value of 180 μm and a maximum value of 800 μm. The mean fibre diameter is about 11 μm. For uniaxial and biaxial mechanical tests tube samples (figure 3) are used, which were provided by a project partner [9] . The design of the sample features geometric stability against buckling due to torsion and compression loads, a high degree of fibre orientation in the z-direction and constant testing conditions for uniaxial as well as biaxial tension, compression and torsion tests. Even though a pin point gate is used for injection moulding, the fibre orientation in the parallel measuring section is almost constant and no pronounced binding line is detected. As a result of the thin wall thickness of 2 mm only a faint centre layer is detected in the measuring section. The plain fibre orientation in the $\varphi - z$-plain averaged through the wall thickness is measured by the nondestructive method of X-ray refraction topography. These results are confirmed by a high resolution computer tomography measurement of a section ($(\Delta r \times \Delta\varphi \times \Delta z) = (2 \times 1 \times 1)\,\text{mm}^3$). The symmetric second order orientation tensor of the spatial fibre orientation which is provided by VG STUDIO MAX (Co. VOLUME GRAPHICS GMBH), indicates a value of 3 % fibre orientation in the direction of wall thickness and 12 % in the circumferential direction. Consequently, the assumption of a plain

fibre orientation distribution in the $\varphi - z$-plain is valid. The two dimensional fibre orientation frequency is described by an elliptic function with the following orientation parameters: $a_{zz} = 0.90$ and $a_{\varphi\varphi} = 0.10$.

4. Experimental setup

The mechanical loading tests are performed on a servo-hydraulic tension-torsion testing machine (CO. INSTRON) which is equipped with a climate chamber (Co.WEISS KLIMATECHNIK GMBH) for regulation of temperature and humidity and the three dimensional optical deformation measurement system ARAMIS (Co. GOM MBH). All tests are performed in the dry material state at room temperature. The frequency of the load controlled fatigue tests is 2 Hz.
For analysing the evolution of micro-damage due to uniaxial and biaxial fatigue loadings the mechanical tests are interrupted after a fixed number of load cycles and offline X-ray refraction analysis is performed (figure 4).

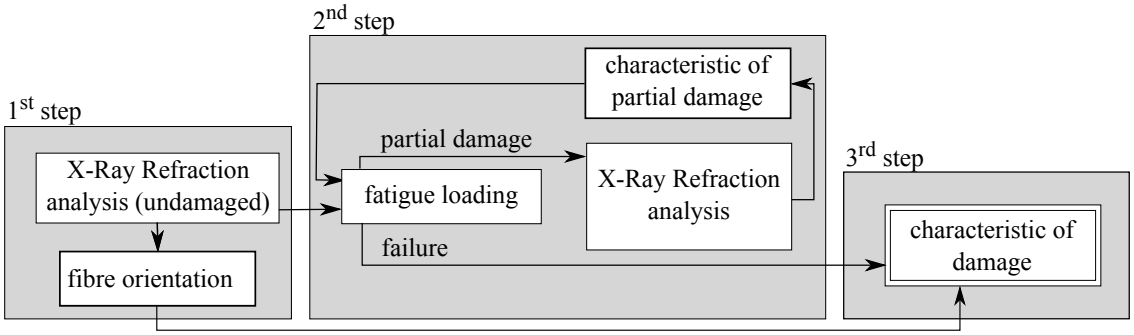

Figure 4. Experimental setup for measuring the damage evolution caused by fatigue loading

5. Results

5.1. Fatigue

For characterizing the fatigue damage behaviour of the PA6 GF30 the load controlled one-step WÖHLER-fatigue test, listed in table 1, are performed. The resultant S-N-curves, shown in figure 5 are calculated by the BASQUIN-equation (eq. 4) for the maximum stresses S_{max} and the amplitudes of stresses S_a respectively. For comparing the curves of different uniaxial and biaxial loadings, a stress approach is used: The maximum stress in the fatigue test is referred to the corresponding static strength.

$$N_F = 10^6 \cdot \left(\frac{S_{max}/R_m}{S_E/R_m} \right)^{-k} \qquad N_F = 10^6 \cdot \left(\frac{S_a/R_m}{S_E/R_m} \right)^{-k} \tag{4}$$

In the biaxial tests (ratio of biaxiality $\lambda_B = \sigma/\tau = 1$) the axial and torsional components of stress are related to the biaxial values of static strength.
With the following assumptions the TSAI-HILL-criterion (eq. 5) is used for connecting the uniaxial strength data with the biaxial strength data:

- Transversely isotropic behaviour, due to the high degree of fibre orientation in the direction of the samples centre line
- Plane stress state as a result of the thin wall thickness

$$F_{static} = \left[\left(\frac{\sigma_{zz}}{R_{m,zz}}\right)^2 - \frac{\sigma_{zz}\cdot\sigma_{\varphi\varphi}}{R_{m,zz}^2} + \left(\frac{\sigma_{\varphi\varphi}}{R_{m,\varphi\varphi}}\right)^2 + \left(\frac{\tau_{z\varphi}}{R_{m,\varphi z}}\right)^2\right] = 1 \tag{5}$$

The TSAI-HILL-criterion implies identical strength behaviour for positive and negative axial stresses, since this does not fit to the analysed material a separate calculation for tension and pressure is required. By substituting the strength data in (eq. 5) with fatigue data the TSAI-HILL-criterion is applied to the fatigue tests (eq. 6) and (eq. 7) (figure 6).

$$F_{fatigue} = \left[\left(\frac{\sigma_{zz}}{S_{max,zz}(N)}\right)^2 - \frac{\sigma_{zz}\cdot\sigma_{\varphi\varphi}}{(S_{max,zz}(N))^2} + \left(\frac{\sigma_{\varphi\varphi}}{S_{max,\varphi\varphi}(N)}\right)^2 + \left(\frac{\tau_{z\varphi}}{S_{max,z\varphi}(N)}\right)^2\right] = 1 \tag{6}$$

$$S_{max,ij} = S_{E,ij}(N = 10^6)\cdot\left(\frac{10^6}{N}\right)^{(-k_i)^{-1}} \qquad i,j = zz,\varphi\varphi,\varphi z \tag{7}$$

In figure 5 all S-N-curves are displayed in one diagram. The corresponding fatigue data are

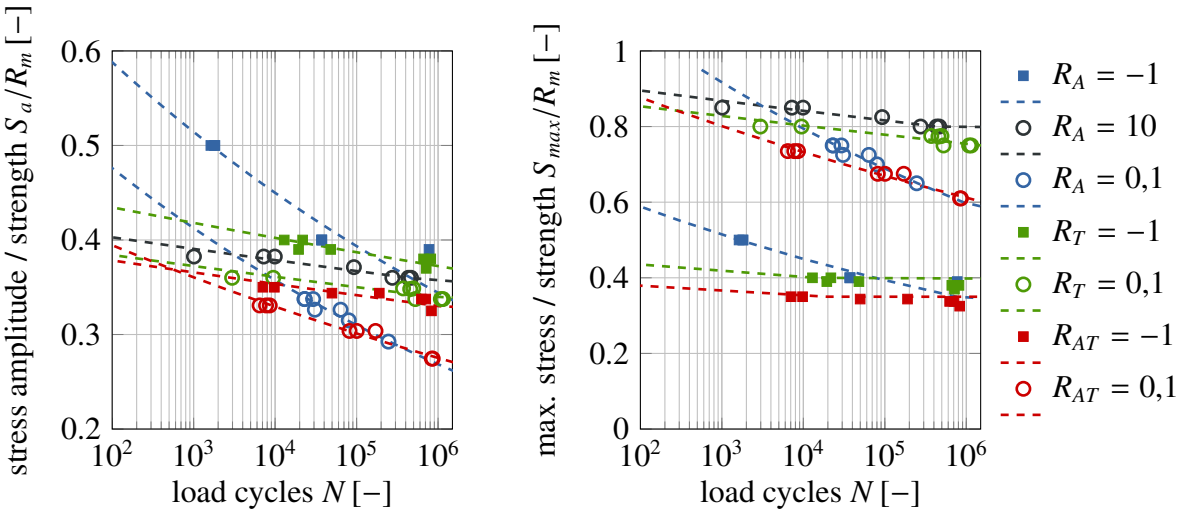

Figure 5. S-N-curves: stress amplitude (left), maximum stress (right)

summarized in table 1. It is shown that the fatigue behaviour is sensitive to amplitude of stress. All S-N-curves reach the endurance limit of 10^6 load cycles between 28 % and 37 % of the corresponding strength value (figure 5, left).
In figure 6 the static strengths and fatigue strengths for defined load cycles to failure N_F are displayed in the failure curve of the TSAI-HILL-criterion. For the biaxial static strengths and the fatigue strength ($R = 0.1$) the criterion yields a conservative estimation. For the biaxial fatigue tests with a load ratio of $R = -1$ the range of high cycle fatigue is quite small. Hence the TSAI-HILL-criterion yields a conservative estimation for the lower load levels and an unsafe estimation for the higher load levels. Nevertheless the TSAI-HILL-criterion is a satisfying way to describe the biaxial fatigue behaviour of PA6 GF30.

load	**S-N-curve**	$k\,[-]$	$S_{E,max}/Rm\,[-]$	$S_{E,a}/R_m\,[-]$
axial	$R_A = -1$	17.2	0.34	0.34
torsional	$R_T = -1$	59.6	0.37	0.37
axial-torsional	$R_{AT} = -1$	67.6	0.33	0.33
axial	$R_A = 0.1$	16.1	0.60	0.27
axial	$R_A = 10$	74.4	0.79	0.36
torsional	$R_T = 0.1$	74.5	0.75	0.34
axial-torsional	$R_{AT} = 0.1$	25.6	0.61	0.28

Table 1. Results of the WÖHLER-fatigue tests. k: slope of S-N-curve, $S_{E,max}/R_m$ load level regarding maximum stress at endurance limit, $S_{E,a}/R_m$: load level regarding stress amplitude at endurance limit

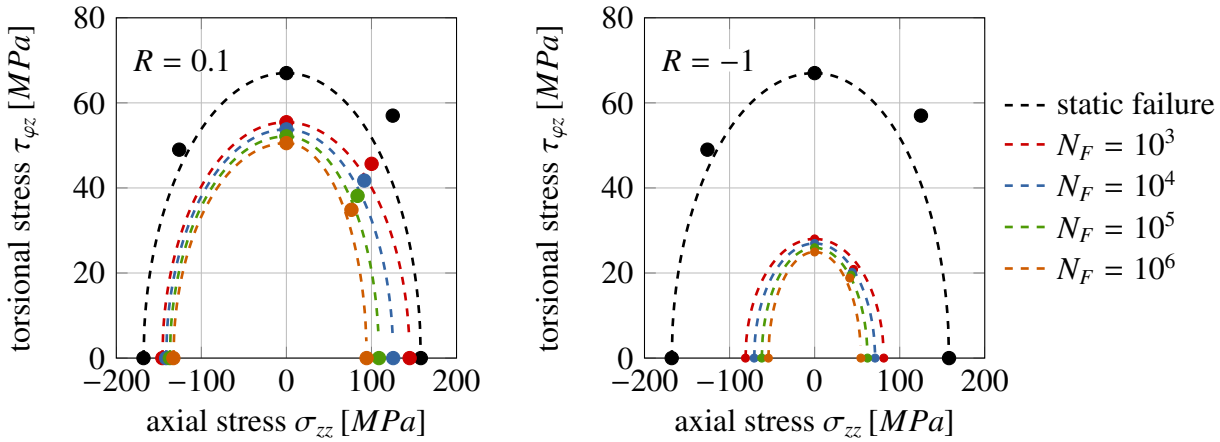

Figure 6. Static and fatigue damage curves from TSAI-HILL-failure-criterion (− − model, • experimental result): Load ratio $R = 0.1$ (left) and $R = -1$ (right).

5.2. Damage evolution

The damage evolution of fatigue loaded ($R = 0.1$) samples under pure axial and torsion load is characterised by the nondestructive method of X-ray refraction analysis. The model for separating the micro damage phenomena of fibre-matrix-debonding and matrix-micro-cracking is introduced by GÜNZEL in [1].
Further examination of the evolution of strains in the fatigue tests reveal that the amplitude of strain is constant whereas the average strain increases with the number of load cycles. This behaviour is ascribed to the process of creeping. Plotting the damage phenomena matrix-cracking and fibre-matrix-debonding to the mean value of creep strain a linear correlation between the creep strain and damage level is shown (figure 7). In detail it is pointed out that the torsion fatigue load causes a considerable higher level of fibre matrix debonding ($\approx$ 15 %) than the axial fatigue load ($\approx$ 8 %). Regarding the density of inner surfaces (matrix-micro-cracking) the relation is inverse: The axial fatigue loaded samples reach a twice higher value of the density of inner surfaces ($\approx 0.5\,\mathrm{mm}^{-1}$) then the torsion loaded samples ($\approx 0.25\,\mathrm{mm}^{-1}$).

$$\varepsilon_m = \varepsilon_{m,\,linear\,elastic} + \varepsilon_{m,\,creep} \qquad \text{for axial strain and} \tag{8}$$

$$\gamma_m = \gamma_{m,\,linear\,elastic} + \gamma_{m,\,creep} \qquad \text{for shear strain} \tag{9}$$

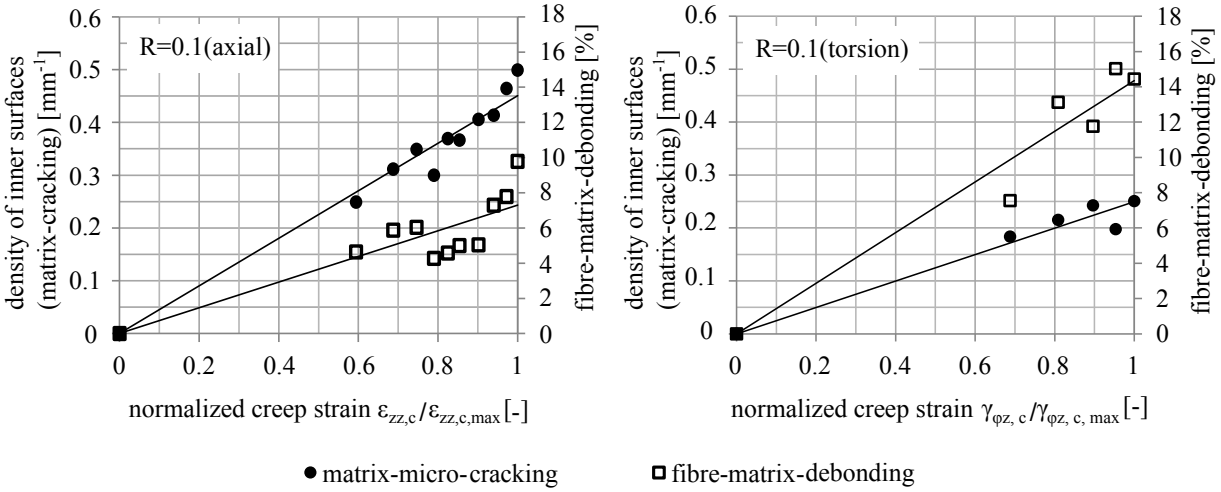

Figure 7. Damage evolution as a result of fatigue loading ($R = 0.1$): Tension loading (left) and torsion loading (right)

6. Conclusion

In this paper our results regarding the uniaxial and biaxial fatigue behaviour and the damage evolution caused by fatigue loading of a PA6 GF30 are presented.
The WÖHLER-tests with the load ratios of $R = 0.1$, $R = 10$ and $R = -1$ show a similar sensitiveness regarding the amplitudes of stress. The application of the TSAI-HILL-criterion to the static strength data and the fatigue data results in a save estimation of the biaxial behaviour regarding static strength values and fatigue under the load ratio of $R = 0.1$. Only for higher load levels of the load ratio $R = -1$ the determination is unreliable.
The evolution of fatigue damage of pure tensile and pure torsion loaded samples is shown. A linear correlation between the creep strain and the damage level is determined. Furthermore it is shown that the level of the occurring damage phenomenon depends on the load type: Axial fatigue loading ($R = 0.1$) causes a higher level of fibre matrix debonding whereas the damage caused by torsional fatigue loading ($R = 0.1$) is dominated by fibre-matrix-debonding.

7. Acknowledgement

The research, presented in this paper is funded by the German Federal Ministry of Economics and Technology in the ZIM-program (support code: KF2201017HAO). Further, we would like to thank our project partner INPRO GMBH, the colleagues of BAM-8.5 MICRO NDE for supporting us with high resolution computer tomography measurements and the DAAD for financially supporting the author's participation at the ECCM 16

References

[1] S. Günzel. Zur quantitativen Analyse des Schädigungsverhaltens eines kurzglasfaserverstärkten Polyamids unter mechanischer Belastung mittels Röntgen-Refraktionsanalyse, Bruchmechanik und Fraktographie. Diss., TU Berlin, 2012.

[2] V. Trappe, S. Günzel, and S. Hickmann. Non-destructive evaluation of micro cracking in short fibre reinforced thermoplastics with x-ray-refraction. In *Int. Conf. on Composite*

Materials (2009) Edingburgh, 2009.

[3] M. P. Hentschel, R. Hosemann, A. Lange, B. Uther, and R. Brückner. Röntgenkleinwinkelbrechung an Metalldrähten, Glasfäden und hartelastischem Polyproplen. *Acta Crystallographica Section A Foundations of Crystallography*, 43(4):506–513, July 1987.

[4] M.P. Hentschel, K.-W. Harbich, and A. Lange. Nondestructive evaluation of single fibre debonding in composites by x-ray refraction. *NDT & E International*, 27:275–280, 1994.

[5] M.P. Hentschel, A. Lange, K.-W. Harbich, D. Ekenhorst, and J. Schors. Röntgentopie der Faser- und Polymerorientierung. *Materialprüfung*, 39:121–123, 1997.

[6] K.-W. Harbich, A. Lange, and M.P. Hentschel. Röntgen-Rotations-Refraktometrie. *Materialprüfung*, 37:19–21, 1995.

[7] H.-V. Rudolph, M.P. Hentschel, and H. Ivers. Damage accumulation in short fiber reinforced thermoplast by x-ray refraction. *e-Journal of Nondestructive Testing*, 7, 2002.

[8] Trappe, V., Günzel, S., and Goebbels, J. Modelling the damage behaviour of short fibre reinforced composites using a non-destructively evaluated fibre orientation distribution aand micro cracking. ECCM 15, Venice, 2012.

[9] Kose, K. and Zeiser, A. On the problem of generating reliable material data of SFRPS for structural simulations. ECCM 15, Venice, 2012.